MITSUBISHI ELECTRIC RESEARCH LABORATORIES
http://www.merl.com

Ultrawideband Propagation Channels-Theory, Measurement, and Modeling

Andreas F. Molisch

TR2005-037 May 2005

Abstract

This paper presents an overview of UWB propagation channels. It first demonstrates how the frequency selectivity of propagation processes causes fundamental differences between UWB channels and ”conventional” (narrowband) channels. The concept of pathloss has to be modified, and well-known WSSUS model is not applicable anymore. Next, describe deterministic and stochastic models for UWB channels and identify the key parameters for the description of delay dispersion, attenuation, and directional characterization, and we survey the typical values that have been measured. We also discuss measurement techniques, and methods for extracting model parameters showing that the concepts of narrowband channel parameter estimation (e.g., maximum-likelihood estimation) have to be modified. Finally we discuss the impact of channel models on various UWB systems.

IEEE Transactions on Vehicular Technology

Ultrawideband propagation channels - theory, measurement, and modeling

(invited paper)

Andreas F. Molisch, *Fellow, IEEE* .

This (invited) paper is submitted to
IEEE Transactions on Vehicular Technolgy, special issue on UWB.
To appear fall/winter 2005

Abstract

This paper presents an overview of UWB propagation channels. It first demonstrates how the frequency selectivity of propagation processes causes fundamental differences between UWB channels and "conventional" (narrowband) channels. The concept of pathloss has to be modified, and the well-known WSSUS model is not applicable anymore. Next, describe deterministic and stochastic models for UWB channels and identify the key parameters for the description of delay dispersion, attenuation, and directional characterization, and we survey the typical values that have been measured. We also discuss measurement techniques, and methods for extracting model parameters, showing that concepts of narrowband channel parameter estimation (e.g., maximum-likelihood estimation) have to be modified. Finally we discuss the impact of channel models on various UWB systems.

Index Terms

UWB, channel model, propagation

I. Introduction

Ultrawideband (UWB) signals are defined as signals with either a large relative bandwidth (typically, larger than 20 %), or a large absolute bandwidth (> 500 MHz). This large bandwidth leads to interesting new possibilities for both communications and radar applications. For this reason UWB systems have been investigated for many years. The interest stems mainly from two application areas: UWB radars [1], which are mainly of interest for military applications, and UWB communications systems [2], which also have military applications, but are nowadays mainly driven by commercial applications. UWB communications gained prominence with the groundbreaking work on impulse radio by Win and Scholtz in the 1990s [3], [4], [5], and received a major boost by the 2002 decision of the US frequency regulator (Federal Communications Commission, FCC) to allow unlicensed UWB operation [6]. Since that time, academic, industrial, and military research in that area has abounded (for an overview and further references, see [7], [8], [9]) .

UWB systems show a number of important advantages:

- accurate position location and ranging, due to the fine time resolution [10];
- no significant multipath fading due to fine time resolution [11];
- multiple access due to wide transmission bandwidths [12];
- possibility of extremely high data rates [13];
- covert communications due to low transmission power operation; and
- possible easier material penetration due to the presence of components at different frequencies.

In order to build systems that realize all those potentials, it is first required to understand UWB propagation and the channel properties arising from this propagation. Obviously, the absolute performance of a given system depends on the channel it is operating in - the pathloss is one, but certainly not the only, example of a propagation effect that determines whether a system can perform satisfactorily. But also the system design, and the relative performance of different systems, depend on the propagation channel. As we will detail in Sec. III, the propagation

channel influence such design aspects as construction of the matched filter, choice of the Rake receiver structure, and search algorithms for geolocation of transceivers.

Just like UWB communications, research into UWB propagation channels (for communications application) is a field that is old and young at the same time. One way of interpreting UWB propagation is to consider the propagation of a short pulse through a medium, and its interaction with objects like planes, half-planes, and wedges. Those theoretical investigations have been performed since the days of Sommerfeld at the beginning of the last century; a summary of the history of this work can be found in [14]. However, this theoretical work was not applied to the simulations of typical wireless scenarios until the beginning of the current century, when Qiu analyzed the impact on UWB system design [15]. Furthermore, measurements of UWB propagation channels were performed only in the late 1990s, and the first papers on statistical UWB channel models appeared only in 2001 [16]. Since then, UWB propagation research has gathered more interest. Especially, the standardization activities of IEEE 802.15.3a and 802.15.4a provided industry with an important stimulus. At the same time, many academic researchers have now also identified UWB channels as an interesting topic.

Still, quite a few fundamental questions of UWB propagation are not yet answered in a satisfactory way. Furthermore, the number of measurement campaigns is fairly limited, so that typical propagation parameters for many types of environments (urban outdoor environments, large factory halls, etc.) are unknown. The current paper aims to summarize the current state of the art, as well as to point out gaps in our knowledge, and thus hopefully stimulate research in these areas.

The rest of the paper is organized tas follows: in Section II, we present some background material, especially the frequency regulation and the currently envisioned applications for UWB systems; those determine the frequency range and the environments for which UWB channels are to be explored. The next section describes the frequency dependence of various propagation effects, including free-space propagation, diffraction, and reflection. Section IV then sets up deterministic description methods for UWB channels. Section V establishes a fairly general statistical model that includes pathloss, shadowing, delay dispersion and angular dispersion. Next, we describe the techniques for actually measuring UWB channels, describing aspects of measurement setup, measurement equipment, and methods for extracting the parameters that are specific to UWB. The simplified models and parameter values that have been accepted in standardization are described in Sec. VII. Finally, Section VIII describes the impact of propagation channels on system design. A summary and conclusion wraps up this paper.

II. UWB BACKGROUND

A. Frequency regulations

The first question when investigating UWB channels is the considered frequency range. This, in turn, is determined by the frequency regulations in different countries. Emission of radiation for channel sounding is not admissible outside those ranges; furthermore, commercial interest tends to concentrate on those frequency ranges where UWB products can legally operate. For this reason, the frequency regulations in various countries have an important impact on propagation research.

At the time of this writing, only the frequency regulator in the US, the FCC, has issued ruling concerning UWB emissions. In a report and order [6], it allowed the unlicensed use of UWB devices as long as certain restrictions with respect to the emitted power spectral density are fulfilled. Those "frequency masks" depend on the application and the environment in which the devices are operated. For indoor communications, a power spectral density of -41.3 dBm/MHz is allowed in the frequency band between 3.1 and 10.6 GHz. Outside of that band, no intentional emissions are allowed, and the admissible power spectral density for spurious emissions provides special protection for GPS and cellular services (see Fig. 1). Similarly, outdoor communications between mobile devices is allowed in the $3.1-10.6$ GHz range, though the mask for spurious emissions is different. While not of regulatory concern, the existence of strong emissions by wireless LANs in the 5.1-5.8 GHz band makes this frequency range less attractive for UWB communications.

Several other countries, as well as the ITU (International Telecommunications Union) are currently discussing the admission of license-free UWB transmission. Singapore has allowed a UWB-friendly zone, while Japan probably will issue regulations in the near future. For Europe, the discussion might take somewhat longer, due to the specific regulatory environment. In any case, the frequency range envisioned by those countries is either similar to the one allowed in the USA, or a subset of these.

Some UWB applications are also allowed in the band below 960 MHz. Though those applications place restrictions on the users (e.g., law enforcement or hospitals), the fact that UWB devices are allowed makes this frequency range interesting for propagation research. Furthermore, a number of military UWB systems seem to operate in that range, though exact figures are not publicly available. Military and public-safety applications are usually faced with fewer regulatory constraints than commercial applications.

A further range of restrictions arises from the current technological possibilities. Semiconductor devices are available that cover the whole spectrum assigned to UWB. However, CMOS technology, which is by far the most appealing process for high-volume commercial applications, is currently only available for frequencies up to about 5 GHz. Combined with the problem of emissions by wireless LANs (see above), this leads to a preference of commercial systems for the $3-5$ GHz frequency band for current systems.

Summarizing, we find that UWB propagation modeling is interesting mainly for the $3-5$ GHz range when immediate commercial applications are considered. However, scientific interest, as well as long-term considerations, motivates research for the whole $3-11$ GHz band, as well as $100-960$ MHz.

B. Applications and environments of interest

As a next step, we need to investigate which applications are of interest for UWB communications [17]. These determine the environment in which channel measurements and modeling are of greatest interest, as well as the ranges between transmitter and receiver that should be modeled.

An important application are Personal Area Networks (PANs), where data are transmitted over distances of 10m or less. Among the PANs, we can distinguish between high-data-rate and low data rate applications, with the high

data rate applications (100 Mbit/s and up) mainly related to consumer electronics (digital TV) and computer networks (wireless USB), while low-data-rate applications can include other consumer-electronics applications (e.g., audio streaming), as well as tasks that were traditionally treated by Bluetooth and infrared devices. Irrespective of those data rate considerations, the envisioned environments are mainly office and residential structures, with distances between 1 and 10 m. Both the case of fixed-location devices (e.g., mounted on a TV or PC), and of person-held or body-worn devices are of interest. Note that these two situations lead to greatly differing time-variations of the resulting propagation channels. As mentioned above, all those high-rate applications utilize the $3.1 - 10.6$ GHz range of the spectrum. A special case of PANs are "Body Area Networks" (BAN), where the communication is between two body-worn devices [18]. Due to the short range and the presence of the users body close to both antennas, the propagation conditions for such BANs can be considerably different from other UWB channels.

Another emerging application is sensor networks. As the data rate is much lower (typically 1 kbit/s - 1 Mbit/s), the possible range is considerably larger, namely up to about 100-300m. Applications include monitoring of residential and office environments, plant monitoring, security monitoring at airports and convention centers, as well as outdoor monitoring. Therefore, office environments with large distances between TX and RX, factory halls, airport halls, and outdoor scenarios are all environments of interest. Again, the frequency range $3.1 - 10.6$ GHz is most relevant.

The large bandwidth of UWB systems offers the possibility of high-precision ranging, and therefore geolocation [10]. For this application, the first arriving paths of the impulse response plays a crucial role - this is in contrast to traditional channel measurements and modeling, where quantities like path loss and delay spread are of higher interest. This is true irrespective of the frequency that is used for the transmission of the ranging signals. We will discuss this aspect in more detail in Sec. IV.4.3.

A further application lies in emergency communications, communications by fire departments and law enforcement agencies, and military (tactical) radio [19]. These applications span most of the environments defined above, but also include communications through snow (emergency communications after avalanches), through rubble (e.g., communications with victims after an earthquake), etc. While highly important for these life-saving missions, no published results seem to be available for the channels in those environments at this moment.

III. Frequency dependence of propagation

One of the key differences between UWB propagation channels and conventional channels lies in the frequency dependence of the transfer function. Conventional (narrowband)[1] channels show frequency dependence of the local (or instantaneous) transfer functions due to the different runtimes of multipath components; those variations typically occur within a bandwidth of a few MHz. UWB channels show not only these variations, but also variations of the *averaged* transfer functions; these variations are caused by the different attenuations that different frequency components of the UWB signal encounter. For example, a wall might show a much higher absorption at 10 GHz

[1] In wireless communications, many authors use the term "wideband" for any channel whose transfer function is frequency dependent. We will not use this nomenclature in this paper, but rather call "narrowband" any channel that is not ultrawideband.

compared to 3 GHz. The effect is mainly related to the relative bandwidth of the system. In the following, we will analyze the frequency dependence of different propagation phenomena.

A. Freespace and antennas

The frequency-dependence of the free-space propagation can be found in any textbook on wireless communications: the path gain G_{pr} is given as

$$G_{\text{pr}}(d,f) = \frac{P_{\text{RX}}}{P_{\text{TX}}} = G_{\text{TX}}(f)\eta_{\text{TX}}(f)G_{\text{RX}}(f)\eta_{\text{TX}}(f)\left(\frac{c_0}{4\pi f d}\right)^2 \tag{1}$$

where G_{TX} and G_{RX} are the antenna (power) gains for transmit and receive antenna respectively, and $\eta(f)$ is the antenna efficiency. c_0 is the speed of light, f is the considered frequency, and d is the distance between the antennas. This equation is normally interpreted such that the pathgain decreases with frequency. However, the above formulation also shows us that this is valid only if the antenna gains are constant over frequency. The antenna area $A_{\text{RX}}(f)$ is related to the antenna gain as

$$G_{\text{RX}}(f) = \frac{4\pi f^2}{c_0^2} A_{\text{RX}}(f). \tag{2}$$

The case that either one or both of the antennas has constant antenna area instead of constant gain thus shows a drastically different frequency dependence.

The antenna efficiency is determined mostly by the matching. For most antennas, the bandwidth is defined as the bandwidth over which the desired efficiency can be sustained. However, for UWB antennas, an additional criterion has to be taken into account: frequency variations of the antenna pattern. The importance of this criterion arises from two facts:

1) due to the large relative bandwidth of UWB antennas, the variations of the antenna pattern over the considered frequency range are more pronounced
2) the emission rules for UWB radiation specify that the power spectral density must be limited in each possible direction [6]. This implies that nonisotropic antenna patterns require a reduction of the average power. In other words, the regulations impose a limit on the emitted power in the frequency-angle domain. This aspect has been given little attention in the literature. Most papers on UWB antennas show antenna patterns for different frequencies, but little conscious efforts seems to have been made to make the patterns as uniform as possible over all frequencies.

More details on UWB antennas, as well as further references, can be found in the paper on antennas [REFERENCE TO BE ADDED IN PROOF] in this special issue.

B. Reflection and transmission

Reflection from, and transmission through, dielectric or conductive objects is another important propagation process that shows frequency dependence. Two effects play a major role:

1) the dielectric properties of most materials show significant variations over the frequency ranges of interest. This impacts both the reflection and the transmission coefficients of the considered objects.
2) the transmission through a dielectric layer is governed by the equation [20]

$$T = \frac{T_1 T_2 e^{-j\alpha(f)}}{1 + \rho_1 \rho_2 e^{-2j\alpha(f)}} \tag{3}$$

where T and ρ are the transmission and reflection coefficients, and index 1 denotes air, while index 2 denotes the considered material. The quantity $\alpha(f)$ is the - frequency-dependent - electrical length of the dielectric as seen by waves that are at an angle Θ_t with the layer

$$\alpha = \frac{2\pi}{c_0} f \sqrt{\varepsilon_{\mathrm{r},2}} d_{\text{layer}} \cos(\Theta_\mathrm{t}) \tag{4}$$

where d_{layer} is the (geometrical) width of the layer. A more detailed analysis is given in [21], [22].

A detailed study of the frequency dependence of common building materials was carried out by Virginia Tech [23], [24]. It found that - due to the frequency selectivity of the materials -a pulse sent through various common building materials was considerably distorted, see Fig. 2. This can be interpreted in such a way that the impulse response of a layer of material is not a delta function, but has a finite support. When representing this impulse response by a tapped delay model, the authors found that, e.g., the impulse response of a brick wall extends over 3 taps, and contains less than 90% of the energy in the dominant tap. [25] showed that even in the microwave range, the use of a wide bandwidth still leads to lower total attenuation than for a narrowband signal. Specifically, using $3-5$ GHz bandwidth gives lower attenuation than using a 5 GHz narrowband signal.

C. Diffraction

Another effect that shows a strong frequency dependence is diffraction at the edge of a screen or wedge. It is intuitively clear that the diffraction loss (attenuation in the shadow region) increases with increasing frequency. An example is the canonical problem of diffraction by a half-plane. For a sinusoidal incident field $x_i = A_0 \exp(j\omega t)$, the complex-valued amplitude x of the scattered field at the distance r is given by [14]

$$\begin{aligned} x(j\omega) = u_1 \pm u_2 = A_0 e^{jkr\cos(\varphi-\varphi_0)} F(\sqrt{2kr}\cos(\varphi-\varphi_0)) \\ \pm A_0 e^{jkr\cos(\varphi+\varphi_0)} F(\sqrt{2kr}\cos(\varphi+\varphi_0)) \end{aligned} \tag{5}$$

where $F(x) = \frac{e^{j\frac{\pi}{4}}}{\sqrt{\pi}} \int_x^\infty e^{-j\mu^2} d\mu$ and the plus and minus signs denote the $\mathbf{H}$ and $\mathbf{E}$ polarization of the incident field. φ_0 and φ are, respectively, the incident and observation angles; $k = \omega/c_0$ is the wave number. The directional impulse response can be obtained as [14]

$$\begin{aligned} h_{\text{half-plane}}(\tau,\varphi) = \frac{\sqrt{2r/c_0}}{2\pi} \left[\frac{\cos\frac{1}{2}(\varphi-\varphi_0)}{\tau + (r/c_0)\cos(\varphi-\varphi_0)} \pm \frac{\cos\frac{1}{2}(\varphi+\varphi_0)}{\tau + (r/c_0)\cos(\varphi+\varphi_0)} \right] \\ \times \frac{1}{\sqrt{\tau - r/c_0}} U(\tau - r/c_0) \end{aligned} \tag{6}$$

where $U(t)$ is the unit step function of t. Again, this shows that the impulse response of the diffraction by a screen has a finite support. We furthermore find that the impulse response is different in different directions. This has important implications, as a directional impulse response that cannot be factored into a delay-only part and a angle-dependent only part is more difficult to model and simulate.

A detailed mathematical framework for diffraction by screens as well as wedges and electrically large objects was developed by Qiu in a series of papers; a summary of that work can be found in the book chapter [14].

D. Scattering on rough surfaces

Also reflection by a rough surface shows a strong dependence on the considered frequency [26]. Consider the reflection coefficient from a rough surface. According to the Kirchhoff theory [27], the reflection coefficient ρ is

$$\rho_{\text{rough}}(f) = \rho_{\text{smooth}} \exp\left[-2\left(2\pi \frac{f}{c_0}\sigma_{\text{h}} \sin\varphi_0\right)^2\right], \tag{7}$$

where σ_{h} is the standard deviation of the height distribution, we see immediately the frequency dependence.

IV. Generic channel representations and deterministic channel models

A. Deterministic and stochastic representations

The impulse response of narrowband propagation channels can be represented as the sum of the contributions of the different multipath components (MPCs) [28]. The model would be purely deterministic if the arriving signals consisted of *completely resolvable* echoes from discrete reflectors. However, in most practical cases, the resolution of the receiver is not sufficient to resolve all MPCs. We thus write the impulse response as

$$h(t,\tau) = \sum_{i=1}^{N} a_i(t)\delta(\tau-\tau_i) = \sum_{i=1}^{N'}\sum_{k} \widetilde{a}_{i,k}(t)\delta(\tau-\tau_i) = \sum_{i=1}^{N'} c_i(t)\delta(\tau-\tau_i) \tag{8}$$

where N is the number of MPCs, while N' is the number of resolvable MPCs. The phase of $a_i(t)$ is assumed to vary quickly with time; if the time variations are due to movement of the MS, then a movement by a fraction of a wavelength leads to a significant change. $|a_i(t)|$ and τ_i, on the other hand, vary slowly (movements of the MS over several tens of wavelengths or more are required.

A UWB channel differs in several important respects from that picture:

1) the number of physical MPCs that make up one resolvable MPC is much smaller, due to the fine delay resolution. This has important effects on the small-scale fading statistics, as discussed in Sec. V.F.
2) in a UWB system, the delays τ_i can change noticeably on a much shorter timescale (e.g., due to movements of the MS by a wavelength), see also Sec. VI.B.2.
3) each of the MPCs shows distortions, due to the effects described in Sec. III. Thus, the impulse response must be written as

$$h(t,\tau) = \sum_{i=1}^{N} a_i(t)\chi_i(t,\tau) \otimes \delta(\tau-\tau_i) \tag{9}$$

where $\chi_i(t,\tau)$ denotes the (time-averaging) distortion of the $i-$th echo due to the frequency selectivity of the interactions with the environment.

When considering a deterministic representation of a single impulse response, the pulse distortion does not lead to a fundamental change of the description method. As long as the system is bandlimited, any deterministic impulse response can be represented by a tapped delay line model as long as the tap spacing is at least as dense as required by the Nyquist criterion. One the other hand, the number of taps that is required to represent the impulse response can increase due to the pulse distortion. More importantly, the statistical description changes, as now adjacent taps are influenced by a single physical MPC (see also Sec. III).

A categorization of impulse responses that we will encounter in the subsequent chapters is between "sparse" and "dense" channels. In a sparse channel, MPCs arrive at time intervals that are (sometimes) larger than the inverse of the bandwidth of the considered channel. Thus, not each resolvable delay bin carries a significant amount of energy. Dense models, on the other hand, exhibit interarrival times of the MPCs that are smaller than the resolvable binwidth. As we will discussion in Sec. VIII, this has important consequences for the design of Rake receivers. Whether a power delay profile is dense or sparse depends on two aspects: (i) the considered bandwidth. The larger the bandwidth, the more likely a channel is sparse. (ii) the considered environment. Environments with a large number of reflecting and diffracting objects can lead to dense channels even for extremely large bandwidths. For example, [29] observed dense channels even for 7.5 GHz measurement bandwidth in an industrial environment, while residential environments [30] show sparse behavior at that bandwidth. Especially for sparse channels, the arrival statistics of the MPCs can be observed much more easily than in narrowband channels.

B. Ray tracing for UWB

Ray tracing, i.e., the deterministic solution of Maxwell's equations using high-frequency approximations, has become very popular for channel prediction and network planning. Traditional ray tracing or ray launching follows rays (plane waves that fulfill the narrowband assumption) on their path from transmitter to receiver. Since UWB systems do not fulfill the narrowband assumption, this principle obviously needs to be modified for UWB simulations. One possible approach [31] performs traditional ray tracing at different frequencies, and then combines the results. An alternative computes the impulse responses of the different rays (which depends on the interaction processes they go through) and adds up the contributions from the different rays [32], [33]. [34] used a combination of ray tracing with FDTD.

Refs. [35] and [36] have independently suggested a to combine *deterministic* components that are derived from ray tracing. with a Rayleigh-distributed "clutter" that describes the contributions that stem from diffuse scattering and other propagation paths that are not covered by the ray tracing. For outdoor LOS environments [35], two deterministic components (direct wave and ground wave) are often sufficient, while for indoor environments, [36] have suggested the use of up to three reflections.

V. STATISTICAL CHANNEL MODELS

For the simulation and testing of wireless systems, stochastic channel models are popular [37]. They reflect the essential properties of propagation channels, without trying to emulate the exact behavior for each specific location.

A. Statistical modeling of pathloss exponent

When the received signal power shows fluctuations due to multipath or shadowing, the pathgain in a narrowband system is conventionally defined as

$$G_{\text{pr}}(d) = \frac{E\{P_{RX}(d, f_c)\}}{P_{TX}} \tag{10}$$

where the expectation $E\{\}$ is taken over an area that is large enough to allow averaging out of the shadowing as well as the small-scale fading $E\{.\} = E_{\text{lsf}}\{E_{\text{ssf}}\{.\}\}$, where subscripts "lsf" and "ssf" indicate large-scale fading and small-scale fading, respectively. Due to the frequency dependence of propagation effects in a UWB channel, the wideband path gain is a function of frequency as well as of distance. It thus makes sense to define a *frequency-dependent path gain* (related to wideband path gain suggested in Refs. [38], [39])

$$G_{\text{pr}}(d, f) = E\{\int_{f-\Delta f/2}^{f+\Delta f/2} |H(\widetilde{f}, d)|^2 d\widetilde{f}\} \tag{11}$$

where $H(f, d)$ is the channel transfer function, and Δf is chosen small enough so that diffraction coefficients, dielectric constants, etc., can be considered constant within that bandwidth; the *total* path gain is obtained by integrating over the whole bandwidth of interest.

It greatly simplifies the modeling if we assume that the path gain as a function of the distance and frequency can be written as a product of the terms[2]

$$G_{\text{pr}}(d, f) = G_{\text{pr}}(f) G_{\text{pr}}(d). \tag{12}$$

In that case, the distance dependence of the path gain is the same as in most narrowband channel models. The many results available in the literature for this case can thus be re-used. Specifically, the path gain in dB is usually described by

$$G_{\text{pr}}(d) = G_{\text{pr,0}} + 10n \log_{10}\left(\frac{d}{d_0}\right) \tag{13}$$

where the reference distance d_0 is set to 1 m, and $G_{\text{pr,0}}$ is the path gain at the reference distance. n is the propagation exponent. The propagation exponent also depends on the environment, and on whether a line-of-sight (LOS) connection exists between the transmitter and receiver or not. Some papers even further differentiate between LOS, "soft" NLOS (non-LOS), also known as "obstructed LOS" (OLOS), and "hard NLOS". LOS exponents in indoor environments range from 1.0 in a narrow corridor [40], to 1.2 in an industrial environment [29], to $\sim 1.5 - 2$ in office and residential environments [41], [42], [43], [30], [40]. NLOS exponents typically range from 2 to 2.5 in industrial and outdoor environments [29], [43], 3 to 4 for soft-NLOS in office and residential environments [41],

[2] To our knowledge, no experimental validation of this assumption has been performed yet.

[42], [44] and from 4 to 7 for hard-NLOS in indoor environments [40]. Other papers use a breakpoint model so that the propagation exponent attains a coefficient n_1 up do a breakpoint distance, and n_2 beyond that.

An important refinement of pathloss modeling was introduced by [45] and applied to UWB systems by [46]. In their approach, the pathloss exponent as a random variable that changes from building to building. They found that the probability density function of this random variable can be well approximated by a Gaussian distribution, see Fig. 4. Means and variances of n for LOS and NLOS situations are given in Table II.

The frequency dependence of the path gain is usually given as [47], [48]

$$\sqrt{G_{\text{pr}}(f)} \propto f^{-\kappa} \tag{14}$$

where [36] found κ to lie between 0.8 and 1.4 (including antenna effects), while [49] excluded antenna effects, and then found κ between -1.4 (in industrial environments) and $+1.5$ (in residential environments). It is noteworthy that the coefficient κ can be positive or negative, depending on the environment. It might be useful to model κ as a random variable, which (similar to n) would change from building to building). However, at the moment, there are not sufficient UWB measurements available to parameterize such a stochastic modeling.

Alternative modelings of the frequency dependence of the pathloss include a frequency-dependent pathloss exponent $n(f)$ [50], and and an exponential dependence $\log_{10}\left(PL(f)\right) \propto \exp(-\delta f)$, with δ varying between 1.0 (LOS) and 1.4 (NLOS) [51].

B. Statistical modeling of large-scale fading

Large-scale fading is defined as the variation of the local mean around the pathloss. It is normally modeled to exhibit a lognormal distribution, with a variance of typically $1-2$dB (LOS) and $2-6$dB (NLOS), depending on the environment [29], [43], [44], [30], [42]. Ref. [46] suggested to model the shadowing variance as random variable where distribution (from house to house) is lognormal. The total attenuation due to shadowing and pathloss is thus

$$[G_{\text{pr},0} + 10\mu \log(d)] + [10 n_1 \sigma_\gamma \log_{10} d + n_2 \mu_\sigma + n_2 n_3 \sigma_\sigma] \tag{15}$$

where n_1, n_2 and n_3 are zero-mean, unit-variance Gaussian variables, but with a recommendation to limit n_1 to the range $[-0.75, 0.75]$ and n_2, n_3 to the range $[-2, 2]$ to avoid unphysical values of the attenuation. The other parameters can be found in Table 2.

The large-scale fading is related to diffraction and reflection effects that the MPCs undergo on their way between TX and RX. We conjecture therefore that there could be a frequency dependence of the shadowing (similar to the frequency dependence of the pathloss). However, no experimental investigation of this hypothesis has been done up to now.

C. General shape of impulse response

We next turn our attention to the delay dispersion. It had been recognized in many "narrowband" channel investigations that multipath components tend to arrive in clusters. The most popular way to reflect this mathematically

is the Saleh-Valenzuela (SV) model [52] and its modifications It writes the impulse response as

$$h_{\text{discr}}(t) = \sum_{l=0}^{L} \sum_{k=0}^{K} a_{k,l} \exp(j\phi_{k,l}) \delta(t - T_l - \tau_{k,l}), \tag{16}$$

where $a_{k,l}$ is the tap weight of the k^{th} component in the lth cluster, T_l is the delay of the lth cluster, $\tau_{k,l}$ is the delay of the kth MPC relative to the l-th cluster arrival time T_l. The phases $\phi_{k,l}$ are uniformly distributed, i.e., for a bandpass system, the phase is taken as a uniformly distributed random variable from the range [0,2π]. K is the number of MPCs within a cluster. L is the number of clusters; it can either be assumed fixed [53], or considered to be a stochastic variable [49].

The number of clusters is a function both of the measurement bandwidth, and of the considered environments. Ref. [46] measured mostly one clusters in indoor environments with a measurement bandwidth of 1.25 GHz around a center frequency of 5 GHz; two clusters were found in some special scenarios. Ref. [54] found only one cluster for 2.4 GHz bandwidth around a 5 GHz carrier. Chong et al. found an average of 3 clusters in an indoor residential environments [30] for a measurement bandwidth from 2 to 10 GHz; for similar bandwidths, [43] found an average of 5 clusters in office environments, while [55] found between 1 and 4 clusters in offices and residential areas. For outdoor environments, [44] found up to 14 clusters.

D. Path interarrival times

For the *interarrival times* of the MPCs within a cluster, a number of different models have been proposed:

1) regularly spaced arrival times: this model is suitable for dense channel models. Since the different MPCs are not resolvable, it is easiest to choose all MPCs to lie on a regular grid $T_l + \tau_{k,l} = i\Delta$, where Δ is the sampling interval [56], [29].
2) Poisson arrival times: the most popular model for the arrival times within a cluster is a Poisson process. In a slight abuse of notation, we can write that the probability density function for the arrival of MPC (path) k (given a certain arrival time $\tau_{k-1,l}$ for the previous MPC) is

$$p(\tau_{k,l}|\tau_{k-1,l}) = \lambda_l \exp\left[-\lambda(\tau_{k,l} - \tau_{k,l-1})\right],\ k > 0\ . \tag{17}$$

   where by definition $\tau_{0,l} > 0$. Note that the original SV model assumed that all clusters have the same λ; this is also used in the 802.15.3a channel model, see Sec. VII.A. However, some UWB measurements indicate that the arrival rate is larger for later clusters.
3) Mixed Poisson process: [30] suggest to use mixtures of two Poisson processes as follows

$$\begin{aligned} p\left(\tau_{k,l}|\tau_{(k-1),l}\right) &= \beta\lambda_1 \exp\left[-\lambda_1\left(\tau_{k,l} - \tau_{(k-1),l}\right)\right] \\ &+ (\beta - 1)\,\lambda_2 \exp\left[-\lambda_2\left(\tau_{k,l} - \tau_{(k-1),l}\right)\right],\ \ k > 0 \end{aligned} \tag{18}$$

   where β is the mixture probability, while $\lambda_1$and λ_2 are the ray arrival rates.

The mean interpath arrival times $1/\lambda$ show a wide variation, from 0.18 ns in NLOS situations to more than 20 ns in LOS situations [57]. These variations are caused to a considerable degree by ambiguities of the evaluation procedure, as well as by the impact of the SNR and dynamic range on the results.

E. Cluster powers and cluster shapes

The next step is the determination of the cluster powers and cluster shapes. The most common model for the power delay profile of each cluster is exponential

$$E\{|a_{k,l}|^2\} \propto \Omega_l \exp(-\tau_{k,l}/\gamma_l) \tag{19}$$

where Ω_l is the integrated energy of the lth cluster, and γ_l is the intra-cluster decay time constant. The cluster powers, averaged over the large-scale fading, in general follow an exponential decay

$$10\log(\Omega_l) = 10\log(\exp(-T_l/\Gamma)) \tag{20}$$

The inter-cluster decay time constant Γ is typically around $10-30$ ns, while widely differing values (between 1 and 60 ns) have been reported for the intra-cluster constant γ.

The interarrival times of the clusters are also a Poisson process,

$$p(T_l|T_{l-1}) = \Lambda \exp\left[-\Lambda_l(T_l - T_{l-1})\right],\ l > 0 \tag{21}$$

where Λ is the cluster arrival rate (assumed to be independent of l); $1/\Lambda$ is typically in the range of $10-50$ ns.

The model Eq. (17), (19)-(21) is the classical SV model, as suggested in [52]. It is not only quite simple, but also agrees well with many measurements, and is thus widely used. Still, it does not account for experimentally observed facts:

1) The first component of a cluster can show a stronger power than the one given by Eq. (19). In conventional narrowband modeling, such a strong first component usually occurs only in the first cluster, and can be interpreted as a line-of-sight connection. Several UWB measurements have shown strong specular reflections in later clusters to be the source of strong components for later clusters.
2) The cluster decay rates γ_l depend on the delay of the cluster. A possible solution is to prescribe a linear increase of γ_l with the cluster delay [29]

   $$\gamma_l \propto k_\gamma T_l + \gamma_0 \tag{22}$$

   where γ_0 and k_γ are constants. Furthermore, the decay time constants show a dependence on the distance [46], see also [58]. Furthermore, it can also show random variations from building to building, and even between measurement points within one building [56].
3) The cluster powers show random variations around the value prescribed by Eq. (20). These variations are due to shadowing effects, and thus described by a lognormal distribution. Note that the sum of the cluster powers is the total power, and thus the cluster power variations also determine the variance of the shadowing as described in Sec. V.B.
4) The small-scale-averaged cluster shape is not strictly monotonous, but shows a "fine structure", i.e., deviations from the purely exponential decay. A generalization of Eq. (19) multiplies the power delay profile of Eq. (19) by a random variable $s(\tau_{k,l})$ [46].

5) In some environments, the cluster shape does not show a sharp onset, but rather first a gradual increase until a local maximum is reached, and then a decrease. The following PDP has been suggested for this case:

$$E\{|a_{k,1}|^2\} \propto (1 - \xi \cdot \exp(-\tau_{k,l}/\gamma_{\text{rise}})) \cdot \exp(-\tau_{k,l}/\gamma_1) \tag{23}$$

Here, the parameter ξ describes the attenuation of the first component, the parameter γ_{rise} determines how fast the PDP increases to its local maximum, and γ_1 determines the decay at late times.

It must be stressed that the extraction of SV parameters from measured data is a rather ambiguous procedure. It is often an arbitrary decision whether to consider a (reasonably continuous) power delay profile as a superposition of several closely spaced clusters, or as a single cluster. This has naturally a great impact on the number of clusters as well as the inter-cluster decay time constants. Spatially resolved measurements, like those of [55] are helpful in resolving this ambiguity, as the directions-of-arrival offer an additional domain from which to determine whether MPCs are clustered or not.

None of the discussions in this section are inherently tied to specifically ultrawideband properties of the channel. However, the larger measurement bandwidth makes them easier to observe in measurements, and that the impact on system performance might be more significant.

F. Statistical modeling of small-scale fading

We next turn to the variations of the $a_{k,l}$ over a small area, caused by the superposition of unresolvable components. In narrowband systems, many MPCs fall into each resolvable delay bin $[i\Delta, (i+1)\Delta]$, so that the central limit theorem is applicable, and the amplitudes of the bins exhibit a complex Gaussian distribution. In UWB systems, the number of MPCs falling into each resolvable bin is much smaller, and it has been empirically determined that in many environments, alternative amplitude distributions must be used:

- *Nakagami distribution:* was observed in [56], [54], [36], and is given by

$$pdf(x) = \frac{2}{\Gamma(m)} \left(\frac{m}{\Omega}\right)^m x^{2m-1} \exp\left(-\frac{m}{\Omega}x^2\right), \tag{24}$$

  where *m≥1/2* is the Nakagami m-factor, $\Gamma(m)$ is the gamma function, and Ω is the mean-square value of the amplitude. The m-parameter is often modeled as a random variable [56].
- *Rice distribution*: The Rice distribution, which is used in [59] and [36], is well known [60], and describes the envelope of a sum of one dominant component and many smaller components. There is an approximate conversion from Nakagami to Rice distribution [61], though both the low- and the high-amplitude tails show different behavior.
- *Lognormal distribution*: it was suggested for use in UWB by [62]. It is described by

$$pdf_x(x) = \frac{20/\ln(10)}{x\sigma_F\sqrt{2\pi}} \cdot \exp\left[-\frac{(20\log_{10}(x) - \mu_{dB}))^2}{2 \cdot \sigma_x^2}\right] \tag{25}$$

  where σ_x is the standard deviation of F, and μ_{dB} is the mean of the values of x expressed in dB.This distribution has the advantage that the fading statistics of the small-scale statistics and the large-scale variations

have the same form; the superposition of lognormal variables can also be well approximated by a lognormal distribution [61]. Another approach found in the literature is to model the deviations of $|h(\tau)|^2$ around the PDP as lognormal process [46].

- *POCA and NAZU distributions* are distributions for the amplitude created by the superposition of a small number of equal-strength MPCs (POCA), with the possible addition of a strong specular component (NAZU). These distributions were suggested for UWB applications in [63].
- *Weibull distribution*: [51], [64] have suggested to either model the amplitudes, or the deviation of $|h(\tau)|^2$ around the PDP, respectively, by a Weibull distribution.
- *Rayleigh distribution*: for some environments, the Rayleigh distribution is valid even when the resolvable binwidth is very small. For example, [29] observed Rayleigh fading in an industrial environment (many metallic scatterers) even for 7.5 GHz measurement bandwidth.

Several papers have also found that the fading depth increases with increasing delay [56], [59].

Another important aspect is the correlation of the fading at different delays. Such a correlation can occur due to two possible reasons:

1) the WSSUS (wide-sense stationary uncorrelated scattering) model is not valid. The WSSUS model was first introduced by Bello in his seminal paper [65]. It assumes, among other aspects, that fading of resolvable multipath components with different delays is uncorrelated. [65] introduced this model for ionospheric scattering, but it has been widely applied for land mobile radio as well. Several investigations have indicated that its validity is doubtful especially in indoor environments. Physical considerations indicate that the finer the available delay resolution, the worse the validity of the US assumption.
2) per-pulse dispersion occurs. As we have discussed in Sec. III, various propagation phenomena lead to a distortion of each multipath component separately. A single pulse can then influence several adjacent delay bins, which gives rise to correlation of the fading in those bins.

Several experiments have tested fading correlation [56], and did not find a significant amount of correlation in the considered environments. However, further research is needed.

G. Angular dispersion

In addition to the delay dispersion, wireless propagation channels also show angular dispersion. Angular dispersion has drawn much attention recently in the context of multi-antenna systems. However, it also determines the interaction between channels and antennas, in other words, how the physical propagation processes combine with the antenna characteristics to yield the impulse response from antenna terminal to antenna terminal. Narrowband systems model the angular dispersion often by prescribing the azimuth power spectrum APS, i.e., the distribution of the small-scale-averaged power as a function of the direction of arrival (DOA), or the ADPS, where the delay dependence is also taken into account. The APS can usually be modeled as a Laplacian function. For UWB channels, only a small number of angularly resolved measurements is available [66], [55], [36].

The deterministic representation of the double-directional impulse response is similar to that of a narrowband system [67]. However, the statistical description shows some major differences. For narrowband systems, it is common to use a generalization of the WSSUS assumption [68], [69] that states that resolvable components arriving from different directions are independently fading. Just like the "normal" WSSUS assumption breaks down in UWB channels, so does this generalization. Furthermore, the frequency dependence of the propagation processes establishes a link between the delay and the angle of arriving waves: in the case of free-space propagation, a homogeneous plane wave can be described only by a single direction of arrival, but - due to the frequency dependence of the pathloss - impacts several delay bins. For this reason, it is not possible to write the angular delay power spectrum as a product of a PDP and a PAS (an approach that is common in narrowband modeling). A first experimental verification is shown in Fig. 3 of [55], which demonstrates a clear frequency dependence of the angular spread.

H. Temporal variations

There are two possible sources of time variance: movement of the TX or RX (or both), and/or movement of scatterers. If only TX/RX moves, then the Doppler spectrum is related to the APS and the antenna pattern [60]; thus our above discussions about the angular dispersion have consequences for the description of the temporal variations as well.

An even more interesting case occurs when only a single scatterer moves, especially when an object is moving through the (quasi) LOS direction, thus shadowing off the most significant power contribution. In the narrowband case, the simplest way to deal with that situation would be to impose a (time-varying) attenuation of the power of the LOS component. For UWB channels, this model needs to be refined, as the different frequency components propagate around (and through) the obstacle in different ways: in other words, low-frequency components are enhanced. A similar effect occurs when the obstacle shadows off other directions of arrival. Again, these are effects that have been conjectured from physical considerations [70], but no experimental investigations are available that confirm and/or quantify this effect.

When more than one scatterer moves, then the fading statistics become more similar to the case of a moving TX/RX. [64] showed that the variability of the total received signal increases in an indoor environment as more and more persons are moving in a room; however, even with 10 moving persons the variability was not as large as with a moving receiver.

VI. Measurement of channels

A. Measurement techniques

The measurement of UWB channels is more involved than conventional narrowband measurements. The complications arise both from practical considerations, i.e., the requirement of devices with very large bandwidth, and from theoretical difficulties.

1) Measurement devices: The goal of most measurement campaigns is the determination of the impulse response of the channel. In the most simple case, this can be achieved with a pulse sounder, i.e., a device that excites the channel by a short pulse , and the received signal is recorded, e.g., by a sampling oscilloscope. Despite its simplicity, this technique is not in widespread use (see, though, [56], [66]), because of the difficulty of generating short, high-energy pulses, as well as the sensitivity of the measurement to interference from impulsive and narrowband sources.

More robust measurements can be performed with correlative channel sounders, where the transmitter sends out a wideband signal with low peak-to-average signal ratio, and the receiver forms the crosscorrelation of the received signal with the transmit signal. This crosscorrelation is a good approximation to the impulse response if the autocorrelation of the transmit signal approximates a delta function [28]; this is, e.g., the case if the transmit signal is a PN sequence. The delay resolution of such a system is determined by the bandwidth of the transmit signal, e.g., the inverse of the chip duration of the PN sequence. Generating a sequence of very short-duration chips can be even more difficult as generating one short pulse. For this reason, the maximum achievable bandwidth is currently limited to about 3 GHz [54].

The most popular technique uses a vector network analyzer (VNA). Those devices perform the measurement in the frequency domain, by exciting the channel (and measuring at the receiver) with a slowly sweeping (or stepping) sinusoidal waveform. Measurements with a large bandwidth can be performed rather easily; furthermore, inherent averaging in the VNA reduces the sensitivity to interference and noise. On the downside, measurements with a VNA take a long time, which precludes measurements of dynamic changes in the environment, and also hamper the establishment of large (and thus statistically relevant) databases of measurements. Furthermore, modeling of impulse responses is made more difficult by windowing in conjunction with the Fourier transformation into the delay domain. Another issue with VNA measurements is that it requires a cable connection from transmitter to receiver, which restricts the range that can be measured with those devices. This problem can be mitigated by using a *scalar* network analyzer, which measures only the magnitude of the transfer function. The phase is retrieved using a Hilbert transformation. This approach was suggested by [71], who also performed comparisons of this approach with time-domain measurements.

2) Impact of the antennas: UWB antennas have a significant impact on the measurement results. Just like narrowband antennas, they exhibit an antenna pattern that weights the MPCs arriving from different directions. But furthermore, the antenna itself leads to significant distortions of the arriving signal, i.e., the impulse response of the antenna has a support that is larger than the inverse system bandwidth. Finally, this impulse response is different for different directions - this statement is equivalent to stating that the (complex) antenna patterns are different at different frequencies (see Sec. III). This makes the deconvolution of antenna effects and channel effects a highly challenging task.

The deconvolution of channel impulse response and antennas requires a separate computation for the different directions from which the MPCs are incident.[3] It is obvious that this can only be applied if the measurements allow

[3]The first step in such a deconvolution is a calibration measurement of the used antennas in an anechoic chamber. Since both transmit and

in principle the determination of the directions of the MPCs. This is typically achieved by measuring at with a (real or virtual) antenna array instead of with a single antenna. In that case, either Kunisch's de-embedding procedure [72], or the high-resolution SAGE algorithm (see below) can be applied.

Many measurements in the literature do not perform a de-convolution at all, i.e., they present measurement results for the concatenation of a specific antenna with the channel that they have measured. Other papers perform a deconvolution, but ignore the direction-dependence of the antenna impulse response. They determine the PDP as the quotient of the measured PDP with the antenna transfer function in the azimuthal plane, or averaged over all directions. While this greatly simplifies the data evaluation, the impact of this approximation on the accuracy of the measured channel impulse responses is unknown.

It is true in general that the antenna characteristics should vary as little as possible both in the angular and the frequency domain. Even if all the antenna characteristics are known, the noise enhancement inherent in the deconvolution procedures lead to less accurate measurement results.

3) Requirements for measurement setup: Most statistical channel models distinguish between small-scale and large-scale fading. In order to determine the small-scale fading, a sufficient number of measurement points has to be taken in an area where large-scale parameters like shadowing are constant. Experience shows that some 50 measurement points per area are a minimum. The measurement points must be spaced $\Delta x = \lambda/2$ or more apart, to allow the measurement points to experience independent fading (for a small angular spread, larger spacing might be required). The different realizations of the channel can be achieved by moving either the TX and/or the RX. Note that if the measurements are done in the $100 - 1000$ MHz range, it might be difficult to fit 50 measurement points into a small-scale area when only one of the link ends is moved.

Somewhat different requirements arise for the measurement of directional properties of the propagation channel (including the antenna de-convolution described above). In that case, the measurement points should be spaced at most $\lambda/2$ apart, in order to avoid ambiguities of the measured directions of arrival [73]. If the directional properties are to be determined only at the RX, then the multiple measurement locations should be used only at the RX. For both the measurement of the amplitude statistics and for the directional properties it is important that the statistics within the measurement area are stationary. For example, no situation should occur where one measurement point has LOS, while another is shadowed behind an obstacle.

These considerations are valid for any channel measurement. Under normal circumstances, it is thus obvious to select $\Delta x = \lambda/2$, so that both directional information and reliable amplitude statistics can be obtained. What complicates the situation for UWB channels is that in order to properly extract the amplitude statistics, it is required that the measurement points are at least $\lambda_l/2$ apart, where λ_l is the wavelength at the lower band-edge. On the other hand, unambiguous resolution of the directions at all frequencies requires that the measurement points are at most λ_u apart, where λ_u is the wavelength at the upper band-edge. Since λ_l and λ_u can differ by a factor of 3 or more in UWB channels, the conditions are obviously contradictory. The only solution that is strictly valid is to measure

receive antennas impact the measurement results, it is required to either have a reference antenna with known properties, or use two antennas with identical properties.

at points that are λ_u, while at the same time to increase the number of measurement points by a factor of λ_l/λ_u in order to obtain a sufficient number of statistically independent samples. This obviously increases the measurement effort considerably.

In order to determine the effect of shadowing and pathloss, multiple measurements (each of which is done on multiple locations within the small-scale area, as described above) have to be performed. The number of those measurements must be sufficient to extract the shadowing variance and the pathloss law with sufficient statistical reliability. Finally, such a measurement campaign should be performed in multiple buildings (for indoor environments) or widely separated locations (for outdoor environments), in order to determine the variability of pathloss exponent and shadowing variance.[4] Unfortunately, the number of total required measurement points quickly becomes huge, and - especially for VNA-based measurements - the time required to perform the measurement campaigns becomes a major problem.

B. Parameter extraction

1) Extraction of small-scale fading: Statistical channel models need to be parameterized by measurement results. An especially difficult point is the parameterization of the small-scale fading statistics. In narrowband channels, it is common to assume Rayleigh fading, whose parameter (the mean-square value) can be easily obtained from the measurement results. In UWB channels, the question arises which of the various distributions of Sec. V.F best fits the measurement results. A common technique is to perform a hypothesis testing, e.g., a Kolmogorov-Smirnov test, for each of the considered distributions. However, since the considered confidence level, as well as some other parameters of the test, are arbitrary, the result of such a hypothesis testing is of somewhat limited value. In order to improve this situation, Schuster (in [49], [74]) recently suggested to instead use a "model selection" approach.

The large relative bandwidth also causes ambiguities about the delay bins that constitute the ensemble for the amplitude statistics. Consider the case of a line-of-sight component: in order to model its fading statistics, we obviously need to analyze the ensemble of the delay bins (at the different small-scale measurement points) that contain the LOS component. For a measurement area of length L, the runtime of the signal across that area is L/c_0. Thus, the τ_{LOS} can differ by up to L/c_0 at the different measurement points. Runtime of the signal across the measurement area is then not an issue as long as the delay bins are so wide that the index i of the bin into which the LOS falls (i.e., $i\Delta < \tau_{\mathrm{LOS}} < (i+1)\Delta$) is the same irrespective of the measurement location. This is true as long as $LB/c_0 < 1$. Expressing $L = a\lambda$, the condition becomes $aB/f_{\mathrm{c}} < 1$. This is obviously fulfilled for narrowband systems, but violated for UWB systems. It is thus necessary to compensate for the runtime of the LOS component across the measurement area [56]. This compensation is easy, since the direction of the LOS component is known from geometrical considerations.

Taking this argument one step further, the runtime compensation should be done for every multipath component, irrespective of the delay. However, this is very difficult, as the direction of the MPCs with larger delays is not

[4] This aspect, again, is valid for narrowband as well as UWB measurements.

known a priori. Furthermore, the impact of this compensation on the resulting fading statistics might be rather limited; a preliminary investigation by Lund University (unpublished) based on the measurement data of [29] did not find significant changes in the fading depth when runtime compensation was used.

2) High-resolution algorithms: High-resolution algorithms extract the parameters of the MPCs with an accuracy that is better than what could be obtained from a Fourier-based analysis; for example, the delay resolution is better than the inverse bandwidth. These algorithms have attained great popularity in recent years, especially for the directionally-resolved evaluation of narrowband measurement campaigns [37]. While a wide variety of those algorithms is available, only two have been used up to now in the context of ultrawideband systems:

1) the CLEAN algorithm [66] is a serial-interference cancellation algorithm. The basic premise is that the observed signal is a sum of pulses with known shape. The algorithm then first finds the largest pulse by determining the correlation of the received signal with the pulseshape, and identifying the highest peak in that correlation. The contribution of the thus-identified pulse is subtracted from the total signal, and the pulse is correlated with the "cleaned up" signal. This process is repeated until either the energy of the cleaned-up signal falls below a threshold, or each additional iteration step does not lead to a significant reduction of the residual energy.
2) the SAGE algorithm allows an iterative determination of the maximum-likelihood estimate of the parameters of the MPCs [75]. Also SAGE includes an "interference-cancellation" aspect, as contributions from MPCs that are already estimated are subtracted from the considered signal. Depending on the variant of the algorithm, this interference cancellation can be serial or parallel [76]. Note that the original SAGE algorithm makes use of the narrowband assumption, but attempts have been recently made in [77], [78] to extend it to the UWB case.

Both the SAGE and the CLEAN algorithm suffer from a fundamental problem in UWB channels: they assume the validity of a certain data model, and need to know the shape of the arriving pulses, i.e., the convolution of the transmit signal with $\chi_i(\tau)$. If they estimate this function erroneously, then during the interference-cancellation process they subtract a wrong contribution from the total signal. The difference between the subtracted contribution and the "true" contribution from an MPC appears as a "ghost" MPC.

VII. Standardized channel models

A. The 802.15.3a model [79]

The model was developed by the IEEE 802.15.3a standardization group for UWB communications systems in order to compare standardization proposals for high-data-rate wireless PANs. Due to this purpose, the considered environments were office and residential indoor scenarios with a range of less than 10 m. The model is based on measurements of [62], [80]. It distinguishes between four radio environments: LOS with a distance between TX and RX of $0-4$m (CM1), NLOS for a distance $0-4$m (CM2), NLOS for a distance $4-10$m (CM3), and a "heavy multipath" environments (CM4).

The model is a "classical" SV model as described in Sec. V.C; the parameters for CM1, CM2 and CM3 were derived from the underlying measurements, while for CM4, the delay spread was set to a higher value (25ns) to cover worst-case situations that are known to occur from other (narrowband) measurements. The extraction of the clusters in the SV model was somewhat ambiguous, as discussed in Sec. V.E, but the channel realizations obtained from the model agree well with the underlying measurement data in terms of rms delay spread and number of significant multipath components.

The large-scale fading is modeled as lognormally distributed, with each cluster undergoing independent shadowing with standard deviation σ_2. The small-scale fading is modeled as lognormally distributed, with a standard deviation of σ_1. As mentioned above, this has the advantage that the small-scale and the large-scale fading are modeled by the same type of distribution. Actually, the underlying measurements do not allow a separation of the observed fading into small-and large-scale fading. For this reason, half of the observed fading depth was ascribed to small-scale fading and large-scale fading respectively, i.e., $\sigma_1 = \sigma_2$. The model does not take into account the pulse distortions that arise from the frequency selectivity of the pathloss and other propagation phenomena.

For each channel realization, the total power of the power delay profile is normalized to unity,[5] and subsequently a "bulk shadowing" is superimposed, i.e., the total impulse response is multiplied with a random variable that is lognormally distributed with a standard deviation σ_{x}. This makes sure that the total PDP shows the correct shadowing distribution, and it is not necessary to compute analytically the interrelationship between the cluster shadowing variance and the bulk shadowing variance.

For the pathloss, the final report of the 802.15.3a channel modeling subgroup recommends the use of the Ghassemzadeh pathloss model $G_{\mathrm{pr}} = G_{\mathrm{pr},0} + 10\mu \log(d) + 10 n_1 \sigma_\gamma \log_{10} d$. However, many simulations use the model in conjunction with a free-space pathloss model $G_{\mathrm{pr}} = G_{\mathrm{pr},0} + 20\log(d)$. While this did not have an impact on the relative performance of the 802.15.3a standardization proposals that were tested with this model, it must be emphasized that the *absolute* performance measures obtained under this assumption are utterly unrealistic for NLOS situations. Other simplifications of the model and their impact on system simulations are discussed in [79].

B. The 802.15.4a model for high frequencies (4a HF) [49]

The 802.15.4a standardization group is currently developing a standard for UWB systems with low data rates and geolocation capabilities for sensor networks. The 802.15.3a models do not cover many of the ranges and environments envisioned for these applications, so that new models had to be developed. In addition, it was decided to take into account several effects that were neglected in the 15.3a models. The resulting model for the $3-10$ GHz range is a generalized SV model, with parameters defined for: residential indoor, office indoor, industrial, outdoor, and farm environments. For each of those environments, LOS and NLOS is distinguished, with the exception of farm environments, where only NLOS situations are modeled. The models are based on measurement campaigns,

[5] Strictly speaking, each $\int |h(\tau)|^2 \mathrm{d}\tau$ is normalized to unity. However, due to the high degree of delay diversity, the impact of the small-scale fading on the integrated energy is very small, so that normalization of $\int |h(\tau)|^2 \mathrm{d}\tau$ and normalization of the PDP is roughly equivalent.

again with the exception of the farm environment, which is based on simulations only. Several of the underlying measurements did not cover the full $3-10$ GHz range, restricting the validity range of the ensuing models.

The pathloss is assumed to depend on distance and frequency according to Eq. (12), with the distance dependence given by (13), and the frequency dependence given by (14); shadowing is *not* included in the model for reasons that are related to the specific simulation requirements in the 15.4a standardization. The impulse response is modeled by a generalized SV model, where the generalizations include:

- the number of clusters is a Poisson-distributed variable; the mean number of clusters is a parameter of the model.
- for some of the environments, the cluster decay time constants are a function of the cluster delay, according to Eq. (22).
- for some NLOS environments (office and industrial), the power delay profile is not exponentially decaying, but rather follows the shape Eq. (23).
- for indoor residential and office environments, the path arrival rates are given by a mixed Poisson distribution, according to Eq. (18). For the industrial environments, the channel model is dense.

The small-scale amplitude distribution is Nakagami, with an m-factor that is independent of the delay, with the exception of the first component, which can have a higher m-factor. The specific parameter values are reported in [49].

In addition to the environments above, also a model for Body Area Networks (BAN) was developed, based on extensive FDTD simulations. It turned out that the results could best be fitted by a model structure that is different from all of the other 15.4a channel models, including the following features: (i) exponential path loss around the body, (ii) correlated log-normal amplitude distributions, (iii) number of clusters fixed to 2, (iv) fixed inter-cluster arrival time, (v) fixed inter-ray arrival time. The model distinguishes three scenarios corresponding to mounting the receiver on the front, side and back of the body (the transmitter is always assumed to be mounted on the front).

The model is based on simulations that include the UWB transceivers and the body only. Recent simulations and measurements in an environment that includes walls and other obstacles indicate a larger number of clusters, with reflections from the walls becoming especially significant of the UWB transceivers are mounted on opposite sides of the body [81]. Further investigations of that topic (see also [18], [82], [83]) thus seem highly important.

C. The 802.15.4a model for low frequencies (4a LF) [49]

In addition to the $3-10$ GHz range, the 802.15.4a group also developed a model for the frequency range from $100-960$ MHz. For this frequency range, only the office NLOS scenario was considered, since this was the only scenario where measurements were available. The chosen model is essentially the model of [56], namely a dense channel model with a single, exponentially decaying cluster. The decay constant is modeled as a deterministic variable that increases with distance as $(d/10m)^{0.5} \cdot 40$ ns (note that this is a deviation from the original model of [56]). This equation gives the same delay spread as the Cassioli model at 10m distance. The distance exponent was chosen as a compromise between the results of Cassioli (no distance dependence) and the results of [58] that

showed a linear increase with distance. The first path has an enhanced amplitude. The path gain follows a simple d^{-n} law according to Eq. (13).

The small-scale fading is modeled by a Nakagami distribution, where the m-parameter is a (truncated) Gaussian random variable, whose mean and variance decrease with delay of the considered delay bin. This can be interpreted that the fading depth increases with delay, since more MPCs fall into a delay bin that has a large delay.

D. Comparison of the models

The crucial differences between the models are the following:

- *dense vs. sparse models:* the 4a LF model, and some of the 4a high-frequency models are dense models, i.e., each resolvable delay bin carriers a significant amount of energy. The 3a models, and some of the 4a HF models, on the other hand, model the arrival times of multipath components as random.
- *strength of the first component:* the 4a LF model always models the first arriving component as the strongest of the power delay profile, irrespective of whether there is a line-of-sight or not.[6] This is not necessarily true for the 3a models; the independent shadowing of the different clusters can cause the maximum of the PDP to be at a larger delay. The 4a industrial and office NLOS PDPs have a weak first component even when no shadowing is present.
- *fading statistics:* different probability density functions are being used: while the 4a LF and HF models use Nakagami distributions, the 3a model uses a lognormal distribution. The 4a LF model uses a delay-dependent fading depth (variance of the fading distribution), while the 4a HF and 3a models assume that the variance that is independent of the delay. Further measurements are necessary to determine whether the difference is really due to different physical behavior in the LF and HF frequency ranges.
- *variations of the delay spread:* for the LF model, the PDP is given by a single-exponential decay. For the HF models, the random variations of the cluster powers due to shadowing (and, in the case of the 4a HF model, the random nature of the number of clusters) lead to a randomization of the delay spread.
- *values of attenuation and delay spread:* the values for the delay spread, and the number of observed clusters, vary significantly between the models. While the 3a model shows delay spreads between 5 and 25ns, the 4a LF model has about 40ns in a similar environment. The 4a HF models show delay spreads up to 100 ns.
- *pulse distortions*: the 3a and the 4a LF models use an impulse response that is a sum of delayed and attenuated delta pulses $\chi_\iota(\tau) = \delta(\tau)$; in other words, the averaged transfer function does not show a frequency dependence. The 4a HF models takes pulse distortions into account, but assumes that the same distortion governs all multipath components, i.e., $\chi_i(\tau) = \chi(\tau)$.

VIII. IMPACT ON SYSTEM DESIGN

In this section, we analyze various UWB transmission schemes that have been proposed in the literature. Due to space restrictions, we do not discuss the schemes themselves, but only mention the impact that the propagation

[6]Note, however, that due to the small-scale fading, the first component of the $impulse\ response$ need not be the strongest.

channel has on their performance.

A. OFDM

OFDM (possibly in conjunction with multiband transmission, see Sec. VIII.B) has been suggested for high-data-rate UWB data transmission [13]. The most significant parameter for OFDM is the *maximum excess delay*, as it determines the length of the cyclic prefix (which in turn determines many other system parameters, see, e.g., [84]). The dependence of UWB-OFDM systems on the delay dispersion thus does not differ significantly from that of narrowband systems - insofar as the delay spread does not depend strongly on the considered bandwidth. Density or sparseness of the impulse response do not have a significant impact.

Finally, systems with a large relative bandwidth offer better resilience with respect to shadowing, as different frequency components see different shadowing coefficients (see Sec. V). This implies that an OFDM system should code the information across different tones in such a way that the resulting frequency diversity can combat the shadowing, as well as the small-scale fading. Frequency diversity can be enhanced by multicarrier-CDMA [85] or pulsed OFDM [86].

B. Multiband principles

In recent years, several schemes have been proposed that divide the available frequency band into subbands, and transmit in different subbands at different times. This approach simplifies implementation, as the sampling and A/D conversion now has to be done only with a rate corresponding to the width of the subband instead of the full bandwidth. The UWB channel is thus converted into a number of narrowband channels, as most propagation effects in a 500MHz channel are in line with conventional (narrowband) propagation. The most significant effect for such systems is the different attenuations that the subbands undergo, see Sec. V.A. The transmit power spectral density has to be constant; so that increasing the power for higher frequencies is not an option; however, stronger coding and/or lower-order modulation can be used to compensate for this effect. Similar to OFDM systems, it is also essential that coding/interleaving across different frequency bands is performed.

C. Rake receivers

For time-hopping impulse radio systems and DS-SS systems, Rake receivers are used for the matched filtering of the received signal. Those structures consist of a matched filter that is matched to the transmit waveform that represents one symbol, and a tapped delay line that matches the impulse response of the channel [87]. This can also be implemented as a number of correlators that are sampled at the delays related to specific multipath components; each of those correlators is called "Rake finger".

For the case that the (instantaneous) channel impulse response can be written as Eq. (8) and the matched filter is matched to the transmit waveform as discussed above, a total of N Rake fingers is required to collect all energy, even in a sparse channel model. If, however, the channel impulse response is described by Eq. (9), the receiver must either have a matched filter that is matched to the convolution of the transmit pulse with the function $\chi(\tau)$ (which

is not feasible in practice, especially if $\chi(\tau)$ is different for each multipath component), or it must use several Rake fingers for each MPC, spaced at the Nyquist sampling distance, to collect the whole energy of this MPC [88], [89]. In the case that the Rake fingers are spaced regularly at delays corresponding to Nyquist sampling, the Rake can implement a filter that is ideally matched to the instantaneous impulse response irrespective of the underlying propagation processes. However, the number of required Rake fingers becomes very large in this case.

But even without those considerations, the fine delay resolution creates a requirement for a large number of Rake fingers. For 7.5 GHz bandwidth, residential environments require on the order of 10 fingers to collect half of the available energy, but that number can increase to 400 fingers in some industrial environments [29].

Due to these problems, several simplified Rake structures have been proposed. It is common to distinguish between $selective$ Rake (SRake) receivers, which collect the energy from the L *strongest* MPCs, and $partial$ Rake (PRake) receivers, which collect the energy from the L *first* MPCs [90].[7] The relative performance of PRake and SRake depends mostly on whether the impulse response is "dense" or "sparse" [90]. For dense channels and monotonous power delay profiles, PRake receivers collect most of the energy, as the taps with the (on average) highest energy are the ones used by the PRake. Of course, sparse channels are more likely if the system bandwidth is large. More detailed investigations in the impact of the bandwidth can also be found in [91].

We also find a significant impact of the amplitude fading statistics. SRakes provide selection diversity, and thus show a steep slope of the BER-vs-SNR curve; PRake receivers do not provide this diversity. However, in channels with small fading depth (e.g., Nakagami-fading with large m-factors), the selection diversity is not needed, so that PRake receivers also show a reasonably steep slope [90].

D. Incoherent receivers

The large number of required Rake fingers has led to an increased interest in incoherent and differentially coherent receiver structures. For AWGN channels, the penalty for the use of incoherent reception is only about 3dB. However, this number increases significantly as the delay spread is increased. The receiver detects the energy over a predetermined time period that is essentially determined by the delay spread of the channel (in order to collect all multipath energy). At the same time, more noise energy is collected. Thus, a large delay spread (which necessitates a large integration time) decreases the performance of incoherent receivers. Sparse impulse responses are especially detrimental, as in the "empty" delay bins, the receiver collects only noise, but no signal energy.

The situation is somewhat similar for transmitted-reference (TR) schemes [92], which transmit an unmodulated reference pulse followed by a modulated data pulse; the receiver multiplies the received signal with a delayed copy of itself, and integrates the resulting signal. The main problem here is noise-noise crossproducts. Sparse channel models lead to an output of a multiplier that has a smaller number of samples with signal energy compared to noise samples; thus the decision variable (output of the integrator after the multiplier) is noisier [93].

A major advantage of the TR scheme is that distortions of the transmit signal (according to the mechanisms of Sec. III) do not significantly influence the performance. The signal that is correlated with the receive signal is the

[7] The *All*-Rake can be seen as the limiting case of either of those structures, collecting all available energy.

reference signal, which has undergone exactly the same distortions as the data pulse.

E. Antenna patterns and multi-antenna solutions

The directional (spatial) characteristics of UWB channels determine the effectiveness of smart antennas and UWB-based MIMO systems, in a way that is very similar to the to conventional multi-antenna systems. One major difference is that beamforming at the transmitter is (for FCC-compliant systems) undesirable, as the restrictions on the transmitted power have to be fulfilled in every direction; directivity thus requires a backoff of the total power. There are, to date, only a few investigations of the directional characteristics of UWB channels [66], [36], [29]. The sample values obtained from these measurements do not yet allow general conclusions about UWB-MIMO system design.

F. Ranging

Geolocation is usually based on ranging, i.e., determining the distance between several nodes [10]. For ranging, it is essential to determine the absolute delay of the $first$ arriving MPC. collecting the energy of subsequent MPCs is not helpful. This task is most easily achieved if the first MPC is the strongest. Most channel models assume that this situation occurs, at least when considering the PDP average over the small-scale fading. For example, the SV model assumes that every cluster has a sharp onset, and the strength of the MPCs within a cluster decreases exponentially with delay. Simulations with such a model will usually result in optimistic estimates of the ranging capabilities. Other models, like the cluster shape Eq. (23), assume a weak first component, while the subsequent components can be stronger.

IX. Summary and conclusions

Just as the interest for UWB systems has intensified in the last years, so has the importance of modeling the UWB propagation channels. Some investigations have pointed out the major differences to existing narrowband models:

- each multipath component can lead to delay dispersion by itself. This effect is especially important for systems with large *relative* bandwidth.
- sparse channels, with significant delays between resolvable MPCs, occur
- the small-scale fading statistics are different, since each resolvable MPC consists of fewer physical MPCs.
- angular and delay characteristics are strongly linked.

The last three issues are mostly important for systems with large *absolute* bandwidth.

We have also outlined the gaps in the current knowledge of UWB channels. Both fundamental questions of propagation mechanisms, measurement and parameter extraction techniques, and statistically reliable parameterizations of channel models are lacking. While the last years have seen significant progress in this field, a lot of research remains to be done before we will possess complete knowledge of this important propagation medium, and its impact on system design.

Acknowledgement: The author's view of UWB channels and their interaction with UWB systems has been shaped by collaborations and discussions with a number of other researchers. In particular, I would like to thank Prof. Moe Win, Dr. Dajana Cassioli, Prof. Robert Qiu, Prof. Larry Greenstein, Dr. Saeed Ghassemzadeh, Dr. Jeff Foerster, Dr. Marcus Pendergrass, Mr. Johan Karedal, Dr. Fredrik Tufvesson, Dr. Chia-Chin Chong, Dr. Kannan Balakrishnan, Dr. Shahriar Emami, Dr. Andrew Fort, Dr. Juergen Kunisch, Mr. Ulrich Schuster, Dr. Philip Orlik, Dr. Zafer Sahinoglou, Dr. Makoto Miyake, and Dr. Jin Zhang. Part of this work was supported by an INGVAR grant from the Swedish Strategic Research Foundation.

REFERENCES

[1] J. D. Taylor, ed., *Introduction to Ultra-Wideband Radar Systems*. Boca Ranton, FL: CRC Press, first ed., 1995.

[2] R. C. Qiu, H. Liu, and X. Shen, "Ultra-wideband for multiple access communications," *IEEE Communications Magazine*, pp. 80–87, 2005.

[3] R. A. Scholtz, "Multiple access with time-hopping impulse modulation," in *MILCOM*, oct 1993.

[4] M. Z. Win and R. A. Scholtz, "Impulse radio: How it works," *IEEE Comm. Lett.*, vol. 2, pp. 36–38, Feb 1998.

[5] M. Z. Win and R. A. Scholtz, "Ultra-wide bandwidth time-hopping spread-spectrum impulse radio for wireless multiple-access communications," *IEEE Trans. Comm.*, vol. 48, pp. 679–691, Apr 2000.

[6] Federal Communications Commission, "First report and order 02-48," 2002.

[7] T. Kaiser (ed.), *UWB communications systems Ű a comprehensive overviewŤ*. EURASIP publishing, 2005.

[8] M. Ghavami, L. B. Michael, and R. Kohno, *Ultra Wideband Signals and Systems in Communication Engineering*. Wiley, 2004.

[9] L. Yang and G. B. Giannakis, "Ultra-wideband communications - an idea whose time has come," *IEEE Signal Processing Magazine*, 2004.

[10] S. Gecizi, Z. Tian, G. B. Giannakis, Z. Sahinoglu, H. Kobayashi, A. F. Molisch, and H. V. Poor, "Localization via ultra-wideband radios," *IEEE Communications Magazine*, in press.

[11] M. Z. Win and R. A. Scholtz, "On the energy capture of ultra-wide bandwidth signals in dense multipath environments," *IEEE Comm. Lett.*, vol. 2, pp. 245–247, Sept 1998.

[12] F. Ramirez-Mireles, "Performance of ultrawideband ssma using time hopping and m-ary ppm," *IEEE J. Selected Areas Comm.*, vol. 19, pp. 1186 –1196, Jun 2001.

[13] A. Batra et al., "Multi-band OFDM physical layer proposal," 2003. Document IEEE 802.15-03/267r2.

[14] R. Qiu, "Propagation effects," in *UWB communications systems Ű a comprehensive overview, T. Kaiser (ed.)*, EURASIP publishing, 2005.

[15] R. C. Qiu, "A study of the ultra-wideband wireless propagation channel and optimum UWB receiver design," vol. 20, pp. 1628–1637, Dec. 2002.

[16] D. Cassioli, M. Z. Win, and A. F. Molisch, "A statistical model for the UWB indoor channel," in *Proc. 53rd IEEE Vehicular Technology Conference*, vol. 2, pp. 1159–1163, May 2001.

[17] D. Porcino and W. Hirt, "Ultra-wideband radio technology: Potential and challenges ahead," *IEEE Communications Magazine*, pp. 66–74, 2003.

[18] I.Kovacs, G. Pedersen, P. Eggers, and K. Olesen, "Ultra wideband radio propagation in body area network scenarios," in *Proc. IEEE ISSSTA 04*, 2004.

[19] R. J. Fontana, "Recent system applications of short-pulse ultra-wideband (uwb) technology," *IEEE Trans. Microwave Theory Techn.*, pp. 2087–2104, 2004.

[20] O. S. Heavens, *Optical properties of thin film solids*. Dover, 1965.

[21] K. Heidary, "Ultra-wideband (uwb) incidence on multiple dielectric interfaces," in *IEEE Antennas and Propagation Society Symposium*, pp. 1315–1318, 2004.

[22] R.Yao, Z. Chen, and Z. Guo, "An efficient multipath channel model for uwb home networking," in *IEEE Radio Wireless Conf.*, pp. 511–516, 2004.

[23] R. Buehrer, W. Davis, A. Safaai-Jazi, and D. Sweeney, "Ultra wideband propagation measurements and modeling - final report to darpa netex program," tech. rep., Virginia Tech, 2004.

[24] A. Muqaibel, A. Safaai-Jazi, A. Bayram, and S. Riad, "Uwb through-the-wall propagation and material characterization," in *2003 IEEE Antennas and Propagation Society International Symposium*, pp. 623–626, 22-27 June 2003.

[25] J. Y. Lee and S. Choi, "Through-material propagation characteristic and time resolution of uwb signal," in *Proc. IEEE UWBST*, pp. 71–75, 2004.

[26] K. W. Lam, Q. Li, L. Tsang, K. L. Lai, and C. H. Chan, "On the analysis of statistical distributions of uwb signal scattering by random rough surfaces based on monte carlo simulations of maxwell equations," *IEEE Trans. Antennas Propagation*, 2004.

[27] R. Vaughan and J. B. Andersen, *Channels, Propagation and Antennas for Mobile Communications*. IEE Press, 2003.

[28] J. D. Parsons, *The Mobile Radio Propagation Channel*. Halstead Press, 1992.

[29] J. Karedal, S. Wyne, P. Almers, F. Tufvesson, and A. F. Molisch, "Statistical analysis of the uwb channel in an industrial environment," in *Proc. VTC fall 2004*, 2004.

[30] Y. K. C. C. Chong and S. S. Lee, "A modified s-v clustering channel model for the uwb indoor residential environment," in *Proc. IEEE VTC spring 05*, p. in press.

[31] H. Sugahara, Y. Watanabe, T. Ono, K. Okanoue, and S. Yarnazaki, "Development and experimental evaluations of "rs-2000" - a propagation simulator for uwb systems," in *Proc. IEEE UWBST 04*, pp. 76–80, 2004.

[32] B. Uguen, E. Plouhinec, Y. Lostanlen, and G. Chassay, "A deterministic ultra wideband channel modeling," in *IEEE Conference on Ultra Wideband Systems and Technologies Digest of Technical Papers*, pp. 1–5, 2002.

[33] A. M. Attiya and A. Safaai-Jazi, "Simlation of ultra-wideband indoor propagation," *Microwvae and optical technology letters*, pp. 103–107, 2004.

[34] G. A. Schiavone, P. Vahid, R. Palaniappan, J. Trace, and T. Dere, "Analysis of ultra-wide band signal propagation in an indoor environment," *Microwave and Optical Technology Letters*, vol. 36, pp. 13–15, 2003.

[35] A. Domazetovic, L. J. Greenstein, N. B. Mandayam, and I. Seskar, "A new modeling approach for wireless channels with predictable path geometries," in *Proc. VTC 2003 fall*, pp. 454–458, 2003.

[36] J. Kunisch and J. Pamp, "Measurement results and modeling aspects for the UWB radio channel," in *IEEE Conference on Ultra Wideband Systems and Technologies Digest of Technical Papers*, pp. 19–23, 2002.

[37] A. F. Molisch and F. Tufvesson, "Multipath propagation models for broadband wireless systems," in *CRC Handbook of signal processing for wireless commmunications* (M. Ibnkahla, ed.), p. in press, 2004.

[38] G. Kadel and R. Lorenz, "Impact of the radio channel on the performance of digital mobile communication systems," in *Sixth IEEE Int. Symp. on Personal, Indoor and Mobile Radio Communications PIMRC'95*, pp. 419–423, 1995.

[39] J.-P. Rossi, "Influence of measurement conditions on the evaluation of some radio channel parameters," *IEEE Trans. on Vehicular Technology*, vol. VT-48, pp. 1304–1316, July 1999.

[40] J. Keignart, J.-B. Pierrot, N. Daniele, A. Alvarez, M. Lobeira, J. L. Garcia, G. Valera, and R. P. Torres, "U.C.A.N. Report on UWB Basic Transmission Loss," Tech. Rep. IST-2001-32710 Ű U.C.A.N., Mar. 2003.

[41] D. Cassioli, W. Ciccognani, and A. Durantini, "D3.1 - UWB Channel Model Report," Tech. Rep. IST-2001-35189 - ULTRAWAVES, Nov. 2003.

[42] A. Durantini, W. Ciccognani, and D. Cassioli, "UWB Propagation Measurements by PN-ŰSequence Channel Sounding," in *Proc. IEEE Int. Conf. on Commun.*, June 2004. Paris, France.

[43] B. Kannan et al., "Uwb channel characterization in office environments," Tech. Rep. Document IEEE 802.15-04-0439-00-004a, 2004.

[44] B. Kannan et al., "Uwb channel characterization in outdoor environments," Tech. Rep. Document IEEE 802.15-04-0440-00-004a, 2004.

[45] V. Erceg et al., "An empirically based path loss model for wireless channels in suburban environments," *IEEE. J. Sel. Areas Commun.*, pp. 1205–1211, 1999.

[46] S. Ghassemzadeh, R. Jana, C. Rice, W. Turin, and V. Tarokh, "Measurement and modeling of an ultra-wide bandwidth indoor channel," *IEEE Transaction on Commun.*, pp. 1786–1796, 2004.

[47] R. Qiu and I.-T. Lu, "Wideband wireless multipath channel modeling with path frequency dependence," in *IEEE International Conference on Communications (ICC'96)*, 1996.

[48] R. C. Qiu and I. Lu, "Multipath resolving with frequency dependence for broadband wireless channel modeling," *IEEE Trans.Veh. Tech.*, 1999.

[49] A. F. Molisch et al., "Ieee 802.15.4a channel model - final report," Tech. Rep. Document IEEE 802.15-04-0662-02-004a, 2005.

[50] D. Cassioli, A. Durantini, and W. Ciccognani, "The role of path loss on the selection of the operating bands of UWB systems," in *Proc. IEEE Int. Symp. on Personal, Indoor and Mobile Radio Communications*, Sept. 2004. Barcelona, Spain.

[51] A. Alvarez, G. Valera, M. Lobeira, R. Torres, and J. L. Garcia, "New channel impulse response model for uwb indoor system simulations," in *Proc. VTC 2003 spring*, pp. 1–5, 2003.

[52] A. Saleh and R. A. Valenzuela, "A statistical model for indoor multipath propagation," *IEEE J. Selected Areas Comm.*, vol. 5, pp. 138–137, Feb. 1987.

[53] S.Venkatesh, J. Ibrahim, and R. M. Buehrer, "A new 2-cluster model for indoor uwb channel measurements," in *Proc. IEEE Antennas Propagation Symp.*, pp. 946–949, 2004.

[54] D. Cassioli and A. Durantini, "A time domain propagation model of the UWB indoor channel in the fcc-compliant band 3.6-6 GHzbased on pn-sequence channel measurements," in *Proc. VTC 04 spring*, 2004.

[55] A. S. Y. Poon and M. Ho, "Indoor multiple-antenna channel charaterization from 2 to 8 GHz," in *Proc. Int. Conference on Communications*, May 2003.

[56] D. Cassioli, M. Z. Win, and A. F. Molisch, "The ultra-wide bandwidth indoor channel: from statistical model to simulations," *IEEE J. Selected Areas Comm.*, pp. 1247–1257, 2002.

[57] D. Cassioli, W. Ciccognani, and A. Durantini, "Uwb channel model report," Tech. Rep. IST-2001-35189-D3.1, 2003.

[58] K. Siwiak, H. Bertoni, and S. M. Yano, "Relation between multipath and wave propagation attenuation," *Electronics Letters*, vol. 39, pp. 142–143, Jan. 2003.

[59] V. Hovinen, M. Hämäläinen, and T. Pätsi, "Ultra wideband indoor radio channel models: Preliminary results," in *IEEE Conference on Ultra Wideband Systems and Technologies Digest of Technical Papers*, pp. 75–79, 2002.

[60] T. S. Rappaport, *Wireless Communications Principles and Practice*. Piscataway, NJ: IEEE Press, 1996.

[61] G. L. Stueber, *Principles of Mobile Communication*. Kluwer, 1996.

[62] J. R. Foerster and Q. Li, "UWB channel modeling contribution from Intel," Tech. Rep. P802.15 02/279SG3a, Intel Corporation, Hillboro, OR, USA, June 2002. IEEE P802.15 SG3a contribution.

[63] H. Zhang, T. Udagawa, T. Arita, and M. Nakagawa, "A statistical model for the small-scale multipath fading characteristics of ultra-wideband indoor channel," in *IEEE Conference on Ultra Wideband Systems and Technologies Digest of Technical Papers*, pp. 81–85, 2002.

[64] P. Pagani and P. Pajusco, "Experimental assessment of the uwb channel variabilityin a dynamic indoor environment," in *Proc. IEEE PIMRC 2004*, pp. 2973–2977, 2004.

[65] P. Bello, "Characterization of Randomly Time-Variant Linear Channels," *IEEE Trans. Comm.*, vol. 11, pp. 360–393, 1963.

[66] R. J.-M. Cramer, R. A. Scholtz, and M. Z. Win, "Evaluation of an ultra-wide-band propagation channel," *IEEE Trans. Antennas Propagat.*, vol. 50, pp. 561–570, May 2002.

[67] M. Steinbauer, A. F. Molisch, and E. Bonek, "The double-directional radio channel," *IEEE Antennas and Propagation Magazine*, vol. 43, pp. 51–63, August 2001.

[68] R. Kattenbach, "Statistical modeling of small-scale fading in directional radio channels," *IEEE J. Selected Areas Comm*, vol. 20, pp. 584 –592, 2002.

[69] B. H. Fleury, "First- and second-order characterization of direction dispersion and space selectivity in the radio channel," *IEEE Trans. Information Theory*, vol. 46, pp. 2027–2044, 2000.

[70] A. F. Molisch, "Time variance for uwb wireless channels," Tech. Rep. Document IEEE 802.15-02-000-00-003a, 2002.

[71] A. Bayram, A. M. Attiya, A. Safaai-Jazi, and S. M. Riad, "Frequency-domain measurement of indoor uwb propagation," in *Proc. IEEE Antennas Propagation Symp.*

[72] J. Kunisch, "Measurement procedures," in *UWB communications systems Ű a comprehensive overview, T. Kaiser (ed.)*, EURASIP publishing, 2005.

[73] H. Krim and M. Viberg, "Two decades of array signal processing research," *IEEE Signal Processing Magazine*, pp. 67–93, 1996.

[74] U. Schuster and H. Boelcskei, "Ultra-wideband channel modeling based on information-theoretic criteria," *IEEE J. Selected Areas Comm.*, p. submitted.

[75] B. H. Fleury, M. Tschudin, R. Heddergott, D. Dahlhaus, and I. K. Pedersen, "Channel parameter estimation in mobile radio environments using the sage algorithm," *IEEE J. Selected Areas Comm.*, pp. 434–450, 1999.

[76] C. C. Chong, D. I. Laurenson, C. M. Tan, S. McLaughlin, M. A. Beach, and A. R. Nix, "Joint detection-estimation of directional channel parameters using the 2-d frequency domain sage algorithm with serial interference cancellation," in *Proc. IEEE ICC 2002*, pp. 906–910, 2002.

[77] K. Haneda and J. I. Takada, "An application of sage algorithm for uwb propagation channel estimation," in *Proc. IEEE UWBST 03*, pp. 483–487, 2003.

[78] K. Haneda, J. I. Takada, and K. Kobayashi, "Experimental evaluation of a sage algorithm for ultra wideband channel sounding in an anechoic chamber," in *Proc. IEEE UWBST 04*, pp. 66–70, 2004.

[79] A. F. Molisch, J. R. Foerster, and M. Pendergrass, "Channel models for ultrawideband personal area networks," *IEEE Personal Communications Magazine*, vol. 10, pp. 14–21, Dec. 2003.

[80] M. Pendergrass and W. Beeler, "Empirically based statistical ultra-wideband (UWB) channel model," Tech. Rep. P802.15 02/240SG3a, Time-Domain Corporation, June 2002. IEEE P802.15 SG3a contribution.

[81] A. Fort, "private comm.," tech. rep., 2005.

[82] T. Zasowski, F. Althaus, M. Stager, A. Wittneben, and G. Troster, "Uwb for noninvasive wireless body area networks: channel measurements and results," in *Proc. IEEE UWBST 03*, pp. 285–289, 2003.

[83] T. B. Welch, R. L. Musselman, B. A. Emessiene, P. D. Gift, D. K. Choudhury, D. N. Cassadine, and S. M. Yano, "The effects of the human body on uwb signal propagation in an indoor environment," *IEEE J. Selected Areas Comm.*, p. 1778Ű1782, 2002.

[84] L. Hanzo, M. Muenster, B. Choi, and T. Keller, *OFDM and MC-CDMA for Broadband Multi-User Communications, WLANs and Broadcasting*. Wiley, 2003.

[85] I. Ramachandran, Y. P. Nakache, P. Orlik, J. Zhang, and A. F. Molisch, "Symbol spreading for ultrawideband systems based on multiband ofdm," in *Proc. PIMRC 2004*, 2004.

[86] E. Saberinia and A. H. Tewfik, "Pulsed and non-pulsed ofdm ultra wideband wireless personal area networks," in *Proc. UWBST 2003*, pp. 275–279, 2003.

[87] M. Z. Win and G. Chrisikos, *Impact of Spreading Badnwidth and Selection Diversity Order on Rake Reception*, ch. 33, pp. 424–254. Prentice-Hall, 2000.

[88] R. C. Qiu, "A generalized time domain multipath channel and its application in ultra-wideband (uwb) wireless optimal receiver design: Wave-based system ananlysis," *Trans. Wireless Comm.*, pp. 2312–2324, 2004.

[89] R. C. Qiu, "A generalized time domain multipath channel and its application in ultrawideband UWB wireless optimal receiver design: system performance analysis," in *Proc. IEEE Wireless Comm. Network. Conf.*, 2004.

[90] D. Cassioli, M. Z. Win, A. F. Molisch, and F. Vatelaro, "Performance of selective Rake reception in a realistic UWB channel," in *Proc. ICC 2002*, pp. 763–767, 2002.

[91] D. Cassioli, M. Z. Win, F. Vatalaro, and A. F. Molisch, "Low-complexity rake receivers in ultra-wideband channels," *IEEE Trans. Wireless Comm.*, p. submitted, 2004.

[92] J. D. Choi and W. E. Stark, "Performance of ultra-wideband communications with suboptimal receivers in multipath channels," *IEEE J. Selected Areas Comm.*, vol. 20, pp. 1754–1766, Dec. 2002.

[93] S. Gezici, F. Tufvesson, and p. y. A. F. Molisch, title=Analysis of transmitted reference schemes for impulse-radio communications booktitle=Proc. Globecom 2004

[94] S. S. Ghassemzadeh, R. Jana, C. W. Rice, W. Turin, and V. Tarokh, "A statistical path loss model for in-home UWB channels," in *IEEE Conference on Ultra Wideband Systems and Technologies Digest of Technical Papers*, pp. 59–64, 2002.

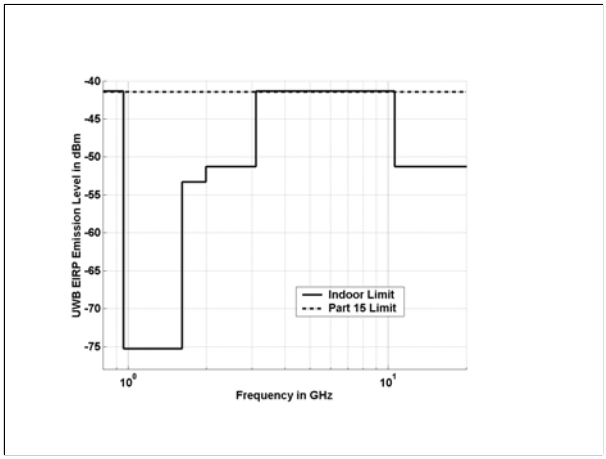

Fig. 1. FCC mask for indoor communications

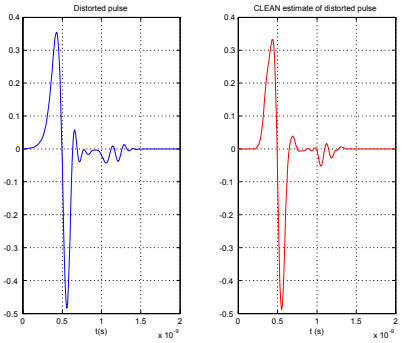

Fig. 2. Distorted UWB Pulse After Passing through Plywood and Pulse Produced from CLEAN algorithm (Sec. VI) with 3-tap model. From [**?**].

environment	range
indoor residential	$1-30$m
indoor office	$1-100$m
body area network	$0.1-2$m
outdoor peer to peer	$1-100$m
outdoor base station scenario	$1-300$m
industrial environments	$1-300$m
emergency communications	$1-50$m

Table I. Typical environments and ranges for UWB applications.

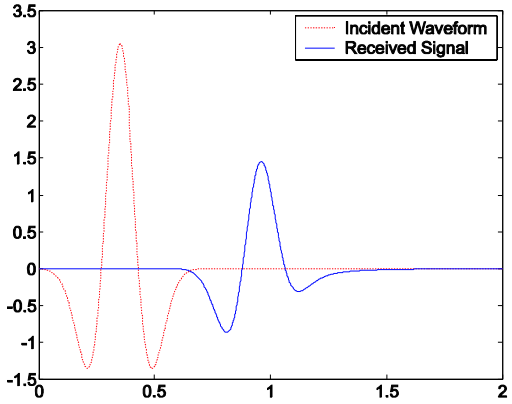

Fig. 3. A UWB pulse is diffracted by a half-plane edge. The received diffracted pulse $r(t) = y_{edge}(t - \tau_3)$ is distorted by the edge where$\tau_3 = 0.92735ns$. The direct path is$\tau_1 = 0.35ns$. The peak amplitude of the diffracted pulse r(t)=w(t) is half of the incident UWB pulse s(t). From [**?**].

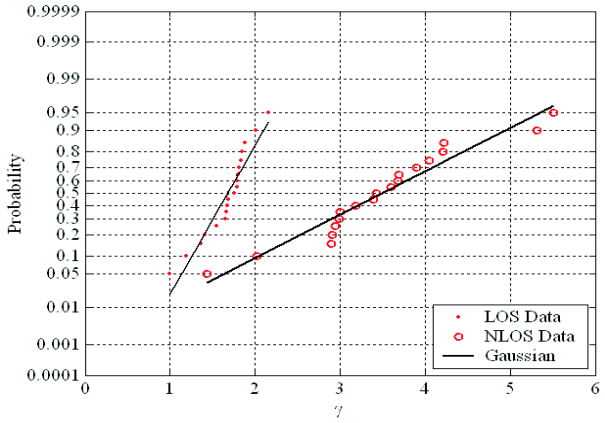

Fig. 4. Cumulative distribution function of the pathloss exponent. From [94].

	Mean	**Std. Dev..**	**Mean**	**Std. Dev.**
PL$_0$ **(dB)**	47	NA	50.5	NA
n	1.7	0.3	3.5	0.97
σ **(dB)**	1.6	0.5	2.7	0.98

TABLE I

PARAMETERS OF THE GHASSEMZADEH PATHLOSS MODEL.

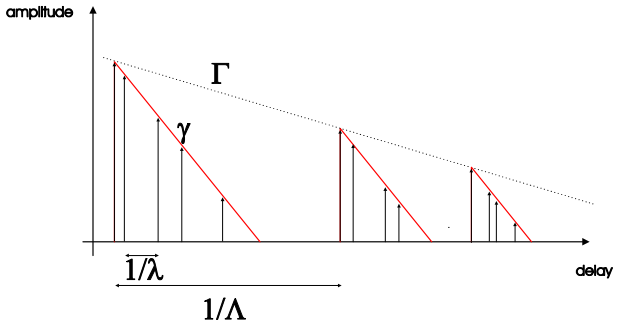

Fig. 5. Principle of the Saleh-Valenzuela model.

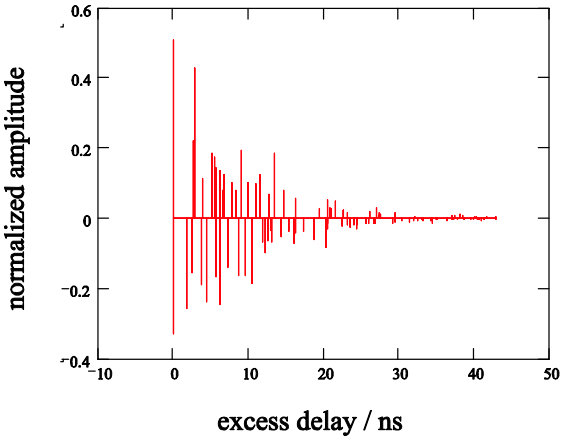

Fig. 6. Realization 17 of Channel Model 1 of the IEEE 802.15.3a standard model.